Title

Mapping the Number of Molecules and Brightness in the Laser Scanning Microscope

Journal

Biophysical Journal, 94(6)

ISSN

0006-3495

Authors

Digman, Michelle A

Dalal, Rooshin

Horwitz, Alan F

et al.

Publication Date

2008-03-01

DOI

10.1529/biophysj.107.114645

Mapping the Number of Molecules and Brightness in the Laser Scanning Microscope

Michelle A. Digman,* Rooshin Dalal,† Alan F. Horwitz,† and Enrico Gratton*
*Laboratory for Fluorescence Dynamics, Department of Biomedical Engineering, University of California, Irvine, California; and †Department of Cell Biology, School of Medicine, University of Virginia, Charlottesville, Virginia

ABSTRACT We describe a technique based on moment-analysis for the measurement of the average number of molecules and brightness in each pixel in fluorescence microscopy images. The average brightness of the particle is obtained from the ratio of the variance to the average intensity at each pixel. To obtain the average number of fluctuating particles, we divide the average intensity at one pixel by the brightness. This analysis can be used in a wide range of concentrations. In cells, the intensity at any given pixel may be due to bright immobile structures, dim fast diffusing particles, and to autofluorescence or scattering. The total variance is given by the variance of each of the above components in addition to the variance due to detector noise. Assuming that all sources of variance are independent, the total variance is the sum of the variances of the individual components. The variance due to the particles fluctuating in the observation volume is proportional to the square of the particle brightness while the variance of the immobile fraction, the autofluorescence, scattering, and that of the detector is proportional to the intensity of these components. Only the fluctuations that depend on the square of the brightness (the mobile particles) will have a ratio of the variance to the intensity >1. Furthermore, changing the fluorescence intensity by increasing the illumination power, distinguishes between these possible contributions. We show maps of molecular brightness and number of cell migration proteins obtained using a two-photon scanning microscope operating with a photon-counting detector. These brightness maps reveal binding dynamics at the focal adhesions with pixel resolution and provide a picture of the binding and unbinding process in which dim molecules attach to the adhesions or large molecular aggregates dissociate from adhesion.

INTRODUCTION

One common and challenging problem in fluorescence microscopy is to determine the average number and brightness (aggregation) of molecules in images. This is a major challenge in cell biology as well, where both the concentration and clustering of proteins can differ in various locations in the cells and change during biological processes. For example, in vitro evidence suggests that membrane receptor aggregation triggers signaling responses. However, few direct demonstrations of aggregation have been reported and none have produced a map of this aggregation with high spatial resolution in vivo.

This determination has become feasible with the pervasive use of fluorescent proteins, and some recent studies have appeared that determine the state of aggregation of proteins in the membrane, the cytoplasm, or in the nucleus of live cells. These approaches use image correlation spectroscopy (1,2), the photon counting histogram analysis (PCH) (3–5), or fluorescence resonance energy transfer (FRET, both homo and hetero) with properly labeled protein partners (6–21). A more common procedure widely used to evaluate the number of molecules in a pixel is to calibrate the fluorescence intensity using a solution of known concentration. This calibration procedure gives the total number of fluorophores, but it cannot provide information on the aggregation state of fluorophores since few bright aggregates or many dim molecules could give the same average intensity.

Using fluorescence correlation spectroscopy (FCS), it is possible to obtain separately the brightness of a particle from the number of particles in a given volume (22) and therefore to determine the degree of aggregation of proteins in solution. This is due to the principle that the occupation number of particles in an open volume follows a Poisson distribution. The ratio of the variance to the square of the average intensity is proportional to $1/N$, where N is the number of particles in the open volume. Once the number of particles has been determined using FCS, the brightness of the fluorescent particle can be obtained by the ratio of the average intensity to the number of particles. This analysis was originally proposed by Qian and Elson for particles in solution and it is known as the ''moment analysis'' (23,24). For homogeneous systems composed of a single molecular species, the moment analysis is sufficient to provide the two quantities of interest, namely the number and brightness of the molecules. A limitation of the moment-analysis is that multiple species of different brightness cannot be resolved using only the first and second moments of the distribution; instead, higher moments are needed, which requires a much larger data set. Recently, a more general approach was proposed, known as the photon-counting histogram analysis

Submitted June 7, 2007, and accepted for publication July 20, 2007.

Address reprint requests to Michelle Digman, Tel.: 949-824-2992; E-mail: mdigman1@gmail.com.

Editor: Alberto Diaspro.

0006-3495/08/03/2320/13 $2.00

doi: 10.1529/biophysj.107.114645

(PCH) (3). The PCH method considers the entire distribution of the photon counts in a given volume rather than only the first and second moments. Since the PCH approach uses the full distribution of photon counts, it is capable of resolving multiple species in a homogeneous solution. This method, originally developed for solutions, has been applied to obtain the state of aggregation of proteins in selected points in a cell, but has not yet been applied to entire fluorescence microscope images (25–27). The PCH method requires a relatively large number of observations at each pixel, and it is computationally too slow for the analysis of all pixels in an image. Therefore, there is a need for a method capable of determining the state of aggregation of proteins simultaneously in the entire cell. If the method is fast (seconds), we could follow the aggregation of proteins in response to external signals and map the state of aggregation across the entire cell.

In this article, we describe the application of the moment analysis to relatively small image stacks. Our purpose is to use this approach to determine the aggregation state of proteins in a given region of the cell. Since the distribution of fluorophores in a cell is not spatially homogeneous and the size of aggregates is unknown, pixel moment analysis could provide a map of this distribution. However, the quantitative interpretation of the measured number of molecules and brightness is not trivial due to the presence of an immobile fraction either from intrinsic cellular features or background fluorescence. In this work, we specifically addressed the effects of the immobile fraction, bleaching, and slowly moving features, which are typical with cellular measurements. The moment analysis can be used in a wide range of concentrations, and it assumes that fluctuations are caused by the occupation number. In a cell, we have regions where proteins are immobile or regions with an autofluorescence or scattering background that contributes to the average intensity but not to the number fluctuations. We found that the ratio of the variance to the average intensity in a pixel is equal to 1 for the intensity fluctuations due to immobile components regardless of the brightness of the immobile features, while it depends on the brightness of the particles for the mobile components. This observation allowed us to separate these two contributions and to measure the brightness of the fast mobile components in the cell independently of the presence of immobile bright features.

We applied moment-analysis to study the process of binding and unbinding of a protein (paxillin-EGFP) to adhesions in CHO-K1 cells. We show that paxillin is monomeric in the cytoplasm but is aggregated when it unbinds from adhesions during disassembly. This is the first time, to our knowledge, that the binding-unbinding process was characterized at high spatial resolution simultaneously in several adhesions in a single cell. The paxillin example shows the potential of the fluctuation analysis performed in parallel using all pixels of an image for biophysical studies of protein-protein interactions in living cells.

MATHEMATICAL BACKGROUND

Characterization of intensity fluctuations

Our approach to obtain the number and brightness of particles at each pixel of the image is based on determining of the first and second moments of the intensity distribution. Given a time series of K-values representing counts k_i obtained during the integration time δt, the first and second moments of the distribution of counts (the average and the variance) are given by

$$\langle k \rangle = \frac{\sum_i k_i}{K}, \tag{1}$$

$$\sigma^2 = \frac{\sum_i (k_i - \langle k \rangle)^2}{K}. \tag{2}$$

These quantities are easily evaluated for any given set of intensity values at each pixel by acquiring successive images in a microscope (although these images need not be successive). It is important to distinguish between the integration time at a pixel and the repetition time of the measurement. For example, in a raster-scan confocal image, each pixel is sampled for a brief period of time, generally in the microsecond range, while the same pixel is resampled when the next frame is acquired. The important parameter is the pixel dwell time, which has to be short enough that the intensity fluctuations are not averaged out, yet long enough to sample fluctuations. In a camera-based system, each pixel is sampled for a time given by the camera exposure time. Therefore, unless cameras with short exposure times are used, the number fluctuations due to fast processes are averaged out while only fluctuations due to slower processes will survive.

Fig. 1 shows schematically the concept of the ratio between the variance and the average intensity. This figure represents the hypothetical intensity at two pixels that have the same average counts (intensity) but different variance. The larger variance at pixel k is due to a few bright particles undergoing number fluctuations while the smaller variance at pixel j is due to many dim particles undergoing fluctuations at that pixel.

Fig. 2 shows schematically the effect of pixel dwell time. In this figure, the autocorrelation function of a solution of fluorescein is shown. At very short autocorrelation lag times (in the microsecond range), the fluctuation is larger than at long autocorrelation time lags (in the millisecond range). Therefore, for molecules undergoing number fluctuations, a long integration time will eliminate the fluctuation.

The Number and Brightness (N&B) analysis

For the derivation of the basic relationships of the Number and Brightness (N&B) analysis, we assume that the variance of the intensity measurement is due to the combination of

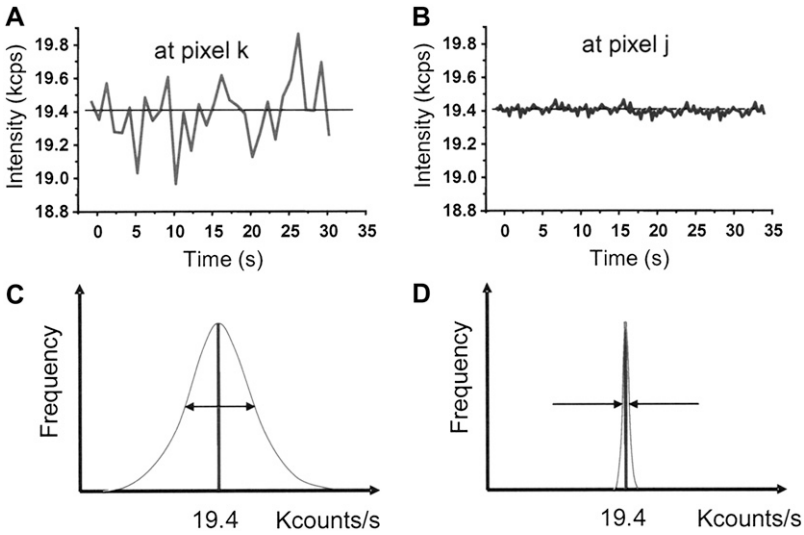

FIGURE 1 At pixels k (A) and j (B) the average intensity is the same but the standard deviation is much larger at pixel k than at pixel j. This is due to few bright particles fluctuating at pixel k while at pixel j there are a large number of dim particles. Panels C and D show schematically the histogram of counts corresponding to the situation in panels A and B, respectively.

two terms, i.e., the variance due to the occupation number (σ_n^2) and the variance due to the count statistics or shot noise (σ_d^2) of the detector. We first ignore other intensity changes in the pixel such as bleaching or slow changes in intensity due to cell movements. We will reintroduce these effects later when we discuss the effect of slowly varying signals and bleaching.

We indicate, with the symbol ε, the molecular brightness defined as the number of photons emitted per second per molecule when the molecule is at the center of the illumination volume. In biological applications, the brightness reflects the clustering or aggregation state of fluorophore-containing molecules. The symbol n indicates the average number of molecules in the illumination volume. The definition of brightness and number of molecules is consistent with the definitions found in Chen et al. (3). Of course, the brightness depends on the laser intensity and the detector sensitivity.

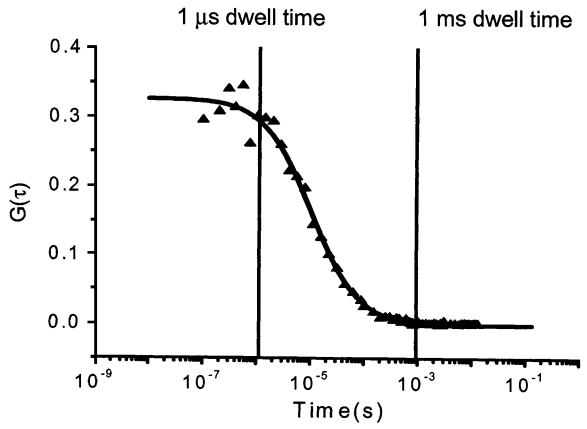

FIGURE 2 Autocorrelation function of fluorescein number fluctuations. Below 10^{-6} s, the amplitude of the fluctuations is large. At 1 ms, the fluctuations have been eliminated.

The variance due to the occupation number is proportional to the square of the molecular brightness and the variance due to the detector is equal to the average intensity (for a photon-counting detector):

$$\sigma_n^2 = \varepsilon^2 n, \tag{3}$$

$$\sigma_d^2 = \varepsilon n, \tag{4}$$

$$\langle k \rangle = \varepsilon n. \tag{5}$$

Equation 3 states that the variance due to number fluctuations depends on the square of the particle brightness. This is a common concept in FCS where each species contributes to the fluctuations according to the square of the particle brightness. Equation 4 states that the detector variance is equal to the intensity. Equation 5 states that the average intensity is the product of the molecular brightness times the average number of particles.

We define the parameter B (apparent brightness) for each pixel as the ratio of the variance to the average intensity and N (apparent number of particles) as the ratio of the total intensity to B,

$$B = \frac{\sigma^2}{\langle k \rangle} = \frac{\sigma_n^2}{\langle k \rangle} + \frac{\sigma_d^2}{\langle k \rangle} = \frac{\varepsilon^2 n}{\varepsilon n} + \frac{\varepsilon n}{\varepsilon n} = \varepsilon + 1, \tag{6}$$

$$N = \frac{\langle k \rangle^2}{\sigma^2} = \frac{\varepsilon n}{\varepsilon + 1}. \tag{7}$$

The value B is related to the brightness ε of the particles, and it is independent of the number of particles. As discussed in the Introduction, B cannot be obtained by a simple calibration procedure based on the intensity of a solution of known concentration. N is directly proportional to the number of particles n. It is easy to extract n and ε from the above equations. We rewrite the above equations in terms of the average intensity and variance,

$$n = \frac{\langle k \rangle^2}{\sigma^2 - \langle k \rangle}, \tag{8}$$

$$\varepsilon = \frac{\sigma^2 - \langle k \rangle}{\langle k \rangle}. \tag{9}$$

When the fluorescence intensity at one pixel is due to the contributions of fluctuating particles plus a constant background fraction there is an additional term to consider before we can obtain the number of fluctuating particles and their brightness. We assume that the background k_0 contributes to the average intensity but does not affect the part of the variance due to the occupation number. Then Eqs. 3–5 become

$$\langle k \rangle = \varepsilon n + k_0, \tag{10}$$

$$\sigma^2 = \varepsilon^2 n + (\varepsilon n + k_0), \tag{11}$$

which, by simple algebra, give the relationships

$$n = \frac{(\langle k \rangle - k_0)^2}{\sigma^2 - \langle k \rangle}, \tag{12}$$

$$\varepsilon = \frac{\sigma^2 - \langle k \rangle}{\langle k \rangle - k_0}. \tag{13}$$

The above expressions are not valid in a pixel where there are only immobile particles since, in this case, $\sigma^2 = \langle k \rangle$ and $\langle k \rangle = k_0$. For cell images we use a map of the ratio $B = \sigma^2/\langle k \rangle$ to determine the parts of the image that have only an immobile fraction. Theoretically, this map will give a value of 1 for each pixel that has only immobile molecules and a value >1 for pixels that contain mobile particles or pixels with additional variance due, for example, to blinking or binding processes. Due to statistics, a value of B close to 1 is obtained with a given error that depends on the number of counts at a given pixel. If all pixels have both mobile and immobile fractions, then the map of B should not have any pixels with a value of 1. However, in the presence of a mixture (in one pixel) of mobile and immobile components, the value of B will be intermediate between 1 and that of the mobile fraction.

Equation 4 is valid for a detector operating in the photon-counting mode. For an analog detector, we must account for the characteristics of the analog amplifier and the settings of the analog-to-digital converter. The moment analysis in the context of analog detectors and cameras will be the subject of a separate publication since there are many additional considerations for these detectors.

After our derivations, the B parameter should always be ≥ 1. However, if the variance is not proportional to the intensity, but there is less variance than that due to the ideal detector, then B will be <1. This condition could happen when the detector or the electronics are saturated as shown in Results.

Presentation of the data

Data will be presented as maps and as one- and two-dimensional histograms. The map of the parameters B and N is very useful for identifying the regions of an image where protein aggregation is occurring. The histogram of the values of B and N is used to quantify the degree of aggregation and to distinguish the presence of aggregates of different sizes and their distribution. Another representation that we found very useful is the two-dimensional histogram (N versus B) representation of pixels of a given value of N and B. This representation identifies regions of a cell with few bright pixels. This representation is also used to estimate the spread of the brightness values.

Simulations

To test the equations derived for the N&B analysis and to test the sensitivity of the proposed method to parameters of the system (such as the number of molecules and their brightness and the number of frames that are needed), we simulated a system of particles diffusing in a box with a given diffusion coefficient. The simulation program is available at our web site (www.lfd.uci.edu), and it has been described elsewhere (28). The diffusion coefficient (10 $\mu m^2/s$) was fast enough so that the fluctuations due to the occupation number will be completed when the same pixel is measured again in the next frame. The pixel dwell time was set at 8 μs and the frame size was 256×256. We simulated a system with different number of particles of the same brightness and a system with the same number of particles of different brightness. We also compared our results with the number of particles recovered with the $G(0)$ obtained by FCS and the brightness as recovered with the PCH analysis method (data not shown).

The results of the simulations are shown in Fig. 3. All pixels of the image (256×256) were averaged to obtain the graphs in Fig. 3. Fig. 3, *A* and *B*, show that the value of B and N calculated according to Eqs. 6 and 7 are linearly proportional to the laser power and to the number of particles, respectively. The calculated value of B according to Eq. 6 is constant, independent of the number of particles over a change in number of greater than a factor of 1000 (Fig. 3 *C*). Fig. 3 *D* shows the effect of increasing the number of frames on the B parameter. When the number of frames is >10, the B-value is recovered correctly. Also the pixel distribution of B versus N is not particularly different between 10 frames and 400 frames (data not shown), implying that under the conditions of the simulations, the pixel-to-pixel variance is relatively small and that B was determined relatively well even using only 10 frames.

We also simulated a system of two molecular species with an identical number of particles differing by a factor of 4 in brightness (data not shown). If the particles are homogeneously distributed, it is impossible by the moment-analysis to separate the two-particle population. The recovered values

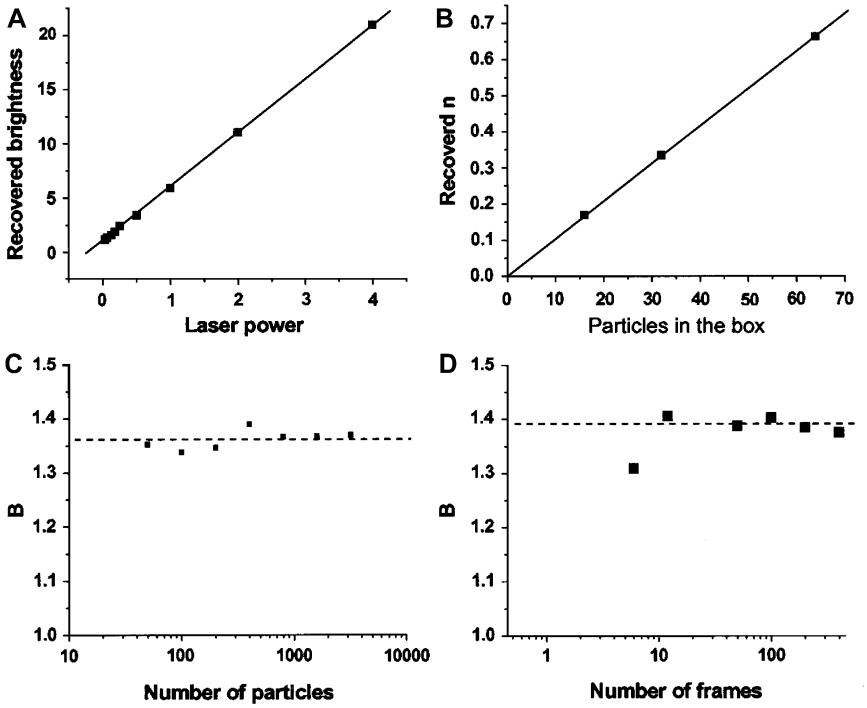

FIGURE 3 Results of simulations. (*A*) Recovered brightness as a function of the laser power. (*B*) Recovered n as a function of the number of particles in the box. (*C*) B as a function of the number of particles. (*D*) B as a function of the number of frames.

for ε tend to emphasize the brighter particles in accordance with the square-law weighting of the brightness discussed in presentation of Eq. 3.

Finally, we simulate a combination of immobile and mobile particles. In this simulation, we have a number of bright fixed beads in a sea of fast diffusion fluorescent molecules. Fig. 4 *A* shows the average intensity image of three beads and mobile particles. Fig. 4 *B* shows the B map calculated at each pixel according to Eq. 6 for this simulation. For the immobile particles, we always obtained a value of $B = 1$. The two-dimensional pixel histogram of the B-value and intensity is shown in Fig, 4, *C* and *E*. The pixels in the B histogram selected by the rectangular areas (*red rectangle*) in Fig. 4, *C* and *E*, are shown in red in Fig. 4, *D* and *E*, respectively. B-values of 1 correspond to the beads, and B values >1 correspond to the mobile particles. In the simulation, we are able to separate the mobile from the immobile fractions.

MATERIALS AND METHODS

Cell culture

CHO-K1 and mouse embryo fibroblast (MEF) cell lines were cultured in minimum essential Dulbecco's Modified Eagle Medium low glucose (1×) (Invitrogen, Carlsbad, CA) supplemented with heat-inactivated 10% (vol/vol) of certified fetal bovine serum (Invitrogen), 50 U/ml penicillin/streptomycin with the exception of the addition of nonessential amino acids added to the CHO-K1 medium. Cells were maintained at 37°C in a humidified chamber with 8.5% or 5% CO_2 for the CHO-K1 and MEF cell lines, respectively. Cells were transfected with plasmids containing GFP and paxillin-GFP using lipofectamine 2000 (Invitrogen) according to manufacturer's protocol. Cells were removed from tissue culture dishes by washing with Dulbecco's phosphate-buffered saline (Invitrogen) without calcium and magnesium followed by 3–5 min incubation with 0.5 mL of trypsin-ethylenediaminetetracetic acid and plated on 35-mm glass bottom dishes (MatTek, Ashland, MA) coated with 1 or 2 μg/ml of fibronectin. Cells were maintained in CCM1 medium (HyClone, Logan, UT) and were imaged 1–2 h after plating. During imaging, cells were kept at 37°C with a Harvard Apparatus chamber (Holliston, MA).

Enhanced green fluorescence protein (EGFP) preparation

Polymerase-chain-reaction amplified, enhanced green-fluorescence protein (EGFP) cDNA (Clontech, Palo Alto, CA) was cloned into the pET-21d vector (Novagen, San Diego, CA) in phase with the 6× His tag region at the C-terminus end. Protein expression was done by transformation of the DNA into BL21(λDE3)-competent cells using ampicillin as a selector. EGFP was then purified to homogeneity by using the Ni-NTA agarose purification system (Qiagen, Valencia, CA). To eliminate all traces of the imidazole in the elution buffer, the purified protein was washed with 20 mM Tris (Sigma, St. Louis, MO) by centrifuging on an Ultrafree-15 centrifugal filter device (Millipore, Billerica, MA).

Two-photon scanning microscopy

Images were taken on a homebuilt, multiscanning microscope as described previously (22). The beam of a Ti:Sapphire 100-fs pulsed laser (Tsunami; Spectra Physics, Newport, CA), mode-locked at 910 nm for EGFP excitation, was coupled through the epifluorescent port of an Axiovert microscope (Zeiss, Maple Grove, MN). The excitation beam was diverted to the sample by a dichroic filter (700DCSPXR; Chroma Technologies, Rockingham, VT). The fluorescence emission was collected using a photomultiplier tube (R7400 series; Hamamatsu, Bridgewater, NJ). An RF amplifier (ACA-4-35-N; Becker & Hickl, Berlin, Germany) and a constant fraction discriminator (model No. 6915; Phillips Scientific, Mahwah, NJ) were used

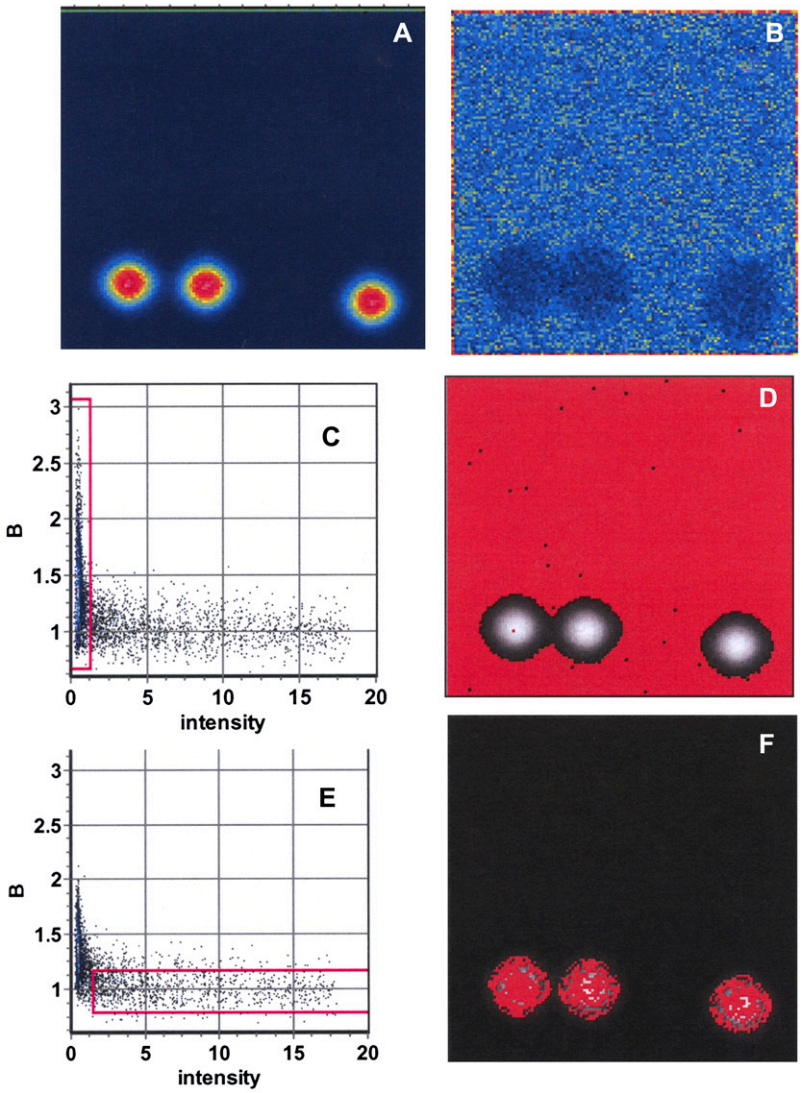

FIGURE 4 Simulation of fixed beads. (*A*) Average intensity image. (*B*) *B* image. (*C*) Selecting regions of the two-dimensional *B*-versus-intensity plot at low intensity and large *B* give the regions colored in red in panel *D* where the beads are absent but fluorescein molecules are present. (*E*) Selecting regions of the two-dimensional *B*-versus-intensity plot at large intensity and *B*-value to ~1 give the regions colored in red (*F*) where the beads are present. Fifty frames were simulated for this figure.

to convert the photon current in TTL electronic pulses. The pulses produced by the discriminator were 8-ns long. The photon pulses were acquired using the ISS-PCI (ISS, Champaign, IL) counter card. A BG39 filter or a ET680SP-2P filter (Chroma Technologies) was placed in the emission path to block the scattered IR. A 40× water immersion objective with a 1.2 N.A. was used for all experiments (Zeiss). For raster-scanned images, the *x*- and *y*-scan mirrors were driven by a three-axis card (ISS) and synchronized with the data acquisition card. All the data acquired was analyzed using the GLOBALS for Images program developed at the Laboratory for Fluorescence Dynamics (UCI, Irvine, CA).

Single-point and raster-scanned images

For single-point FCS, data were collected at the rate of 64,000 Hz. For raster-scanned images, the data were taken at 16 or 32 μs/pixel and between 50 and 100 frames were collected. Images were always acquired at 256 × 256 pixels of a 16 × 16 μm or 32 × 32 μm area so that the pixel size remained 3–4 times smaller than the volume of the point-spread function (Typical waists were ~0.3–0.5 μm depending on the laser wavelength used). The waist of the point-spread function was calibrated daily by measuring the autocorrelation function of 20 nM fluorescein (Invitrogen) in 1 mM NaOH (Sigma) and fixing the diffusion to 300 μm^2/s at 790 nm or using 40 nM EGFP at 910 with a fixed diffusion rate of 90 μm^2/s.

Fixed beads and fluorescein

For the experiments done on the fluorescently labeled polystyrene beads, the wavelength was changed to 790 nm. The beads were diluted in ethanol and sonicated for 2 h. Then a drop of the diluted-bead mixture was placed on a 0.17-mm glass coverslip and allowed to dry for 2 h. An overlay of 100 nM fluorescein was added to the top of the dried beads and images were acquired using the above setup. A piezoelectric *x*-, *y*-, and *z*-nanopositioner (Polytec PI, Auburn, MA) equipped with a transformer feedback sensor was used to drive the stage at 0.002 Hz in the *x*-*y* direction for controlled motion.

Spatial filter

For the analysis of relatively weak emitting samples, we found it necessary to apply a spatial filter to the *B* and *N* maps. We used a filter that is based on convoluting the *B* and *N* images using a median operation. For each pixel, the next-neighbor pixels were analyzed (a 3 × 3 matrix). The value at the

pixel was assigned according to the median value of the matrix. Using this kind of filter, large, isolated fluctuations due to poor statistics are deleted instead of propagating to neighbor pixels which is common in methods using the mean of the matrix rather than the median. This type of filter tends to sharpen the images rather than decrease the resolution. We applied the filter to simulated images, and found that arbitrary clustering of pixels is avoided by this filter.

RESULTS

First we show that, for the detector we are using (in the photon-counting mode), the variance is equal to the intensity. Fig. 5 (slide points) shows the curve of the B parameter (variance/intensity) as function of the intensity for the case in which the detector is illuminated with light from an LED powered by a battery. In this case, there are no fluctuations due to particle movement. The variance is equal to the intensity in a large range of intensities. If we continue to increase the laser intensity, we arrive in a regime where the variance is no longer proportional to the intensity; this is due to the saturation of the detector. For our detector, this regime was reached at $\sim 10^7$ counts/s (Fig. 5). At very low intensity (<1000 counts/s), the variance tends to increase, probably due to contamination from room lights during this experiment. However, this figure shows that in the range of photon flux typical of fluorescence experiments, the B parameter is 1.

Solution data

In Fig. 5 (EFGP points), we show the B parameter obtained by diluting a concentrated solution of EGFP in TRIS buffer. The brightness obtained for this sample using Eq. 6 was 4600 counts/s. Note that the brightness is constant over a wide range of concentrations, from ~ 5 nM to ~ 5 μM. Above 5 μM, the apparent brightness decreases due to the saturation of the detector. This effect was reported previously and the brightness can be corrected using the calibration with the LED illumination experiment (5).

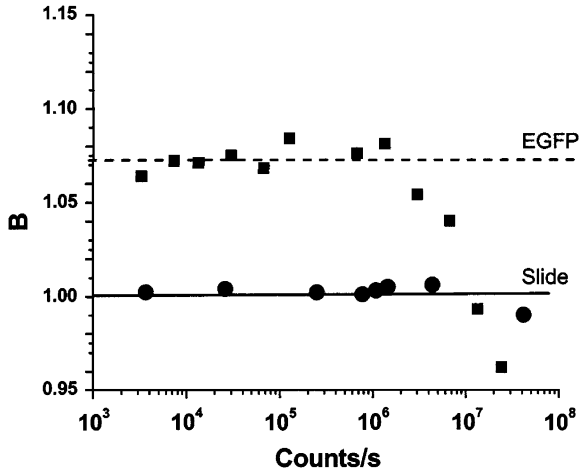

FIGURE 5 B versus intensity for constant illumination (●) and for solutions of EGFP at different concentrations (■). Twenty-five frames were collected for each point in this figure.

A stack of images from a solution of 120 nM EGFP in buffer was collected using different excitation powers. Since the intensity is quadratic with the excitation power, the overall increase in intensity (counts/pixel) was used to evaluate the overall laser power effect. Data were analyzed using Eqs. 8 and 9. A typical two-dimensional histogram of B versus intensity is shown in Fig. 6 *A*. The value of the brightness-versus-sample intensity is shown in Fig. 6 *B*. The average number of particles and brightness for a series of measurements as a function of the protein concentration is shown in Fig. 6, *C* and *D*. The values of the number of particles recovered were in very good agreement with the values obtained by $G(0)$ and the PCH analyses. Note that the spread of the data per each pixel is relatively large (Fig. 6 *A*). However, the average value is recovered with a precision comparable to that of the PCH analysis done using the data from the entire stack. In regard to the map, when we have very few counts we found it necessary to apply a spatial filter (see Materials and Methods) to the average and variance image to further reduce the noise in the determination of n and ε.

Separation of the mobile from the immobile part

One important consequence of the calculation of the B image versus intensity at each pixel is that we should be able to separate the immobile fraction (that has a value of $B = 1$) from the mobile part where B is >1. Furthermore, if we increase the laser power, the mobile part will increase the B-value while the immobile part will remain at $B = 1$. To demonstrate this principle, we prepared a sample of fixed beads immersed in a solution of 100 nM fluorescein at pH = 9. The B image (Fig. 7 *A*) clearly identifies the beads as having low B-values. The two-dimensional histogram of B versus intensity (Fig. 7 *C*) has two branches. One part, corresponding to $B = 1$, maps to the beads while the other part has a value of $B > 1$, and it maps to the solution fraction. When the laser intensity is increased, only the solution part increases the B-value. These results agree with the simulations of fixed beads in a sea of fluorescent molecules.

Correction for bleaching

If the intensity at one location slowly changes due to bleaching, the variance at that location has an extra term in addition to the time change of the average intensity. We assume that only the immobile part bleaches, since bleached, mobile molecules will be replaced with unbleached molecules. This drift of the average intensity can be corrected using different techniques. We have used a high-pass filter technique. The time course is first filtered using a recursive exponential filter with a constant of 10 frames in both directions so that the

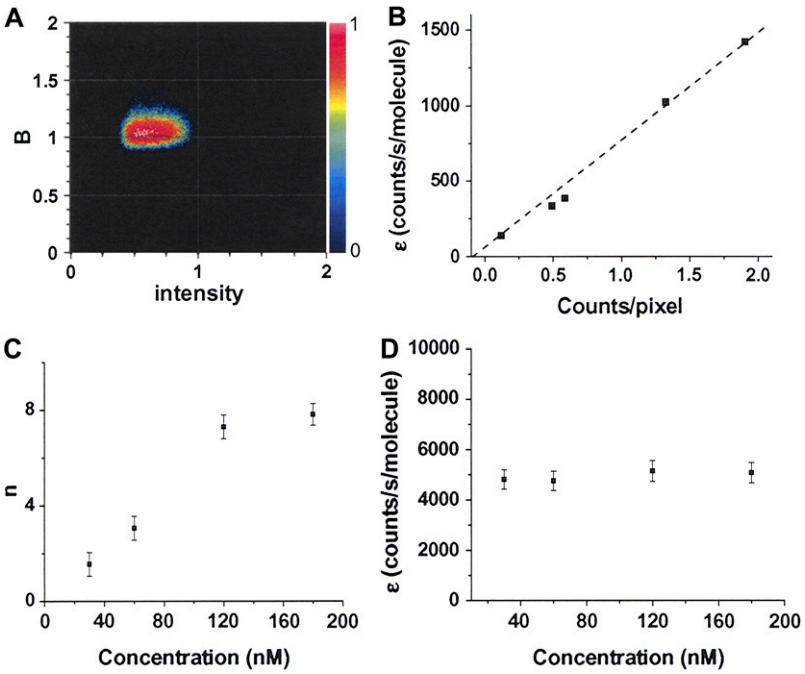

FIGURE 6 (*A*) Typical two-dimensional histogram of *B* versus intensity. The spread of the points in the histogram shows the pixel variance. (*B*) The recovered brightness of a solution of 120 nM EGFP as a function of the laser intensity. The laser intensity was evaluated by the increase in counts of the overall image. (*C*) Recovered number of particles as a function of the EGFP concentration. (*D*) Recovered brightness as a function of protein concentration.

phase of the signal is not changed. We then add a constant equal to the average intensity value at that pixel. The variance of the detrended series is equal to the initial variance due to the high frequency fluctuations, and the average intensity has not changed. Therefore the extra variance of the ''immobile'' part due to bleaching is minimized after correction, and we can recover the variance of the mobile part. The same principle can be applied to slowly moving parts of the image which will give an apparent increase and then decrease of the fluorescence intensity at some pixels.

To prove that the correction for slowly varying parts (either bleaching or slowly moving) is working, we used a sample with the immobile beads immersed in a solution of fluorescein. We increased the laser power until the bleaching of the beads was ~50% during the course of data acquisition. In Fig. 8, we show the effect of bleaching. Without correction for bleaching, the particles have a large variance and they appear bright in the *B* map. After the bleaching correction, the beads are correctly classified as immobile particles with *B* close to 1. We then slowly moved the entire stage, using a piezo driver to simulate the effect of slowly moving cellular features. Also in this case we were able to completely remove the effect of movement from our data, as shown in Fig. 8 *D*.

At this point we have shown that we can correctly recover the number and brightness of particles in solution. We also showed that we can separate the immobile from the mobile fraction in an image and that we can correct for bleaching and slow movements of large ''immobile'' fractions. We note that the basis of our algorithm is to exploit the additional fluctuation due to particles diffusing in and out of the observation volume (the PSF in confocal microscopy). In contrast, the fluctuation approach cannot determine number and brightness separately for the immobile fraction.

Measurements in cells

Cells with uniform brightness components

We acquired a stack of 50 images of a MEF cell transfected with monomeric EGFP. In this system, the EGFP mainly localizes in the cytosol, only weakly interacting with other cellular components. Fig. 9 shows the average intensity image of the stack and the *N* and *B* images. We also show the *B*-versus-intensity two-dimensional histogram. In this system, there is no apparent immobile fraction, and the brightness is relatively constant across the cell; but the apparent number of particles *N* changes accordingly to the cell thickness only at the cell borders.

Cells with molecular aggregates

The power of the N&B method lies in its ability to detect and quantify molecular aggregates. We prepared cells in which we have independently determined the existence of molecular aggregates using single-point FCS or the RICS technique applied to the restricted parts of the cell (29). Fig. 10 shows a CHO-K1 cell expressing paxillin-EGFP. This protein is known to be monomeric in the cytosol and resides in complexes in portions of some adhesions (29). FCS and PCH analysis have shown that when adhesions disassemble in retracting parts of the cell, relatively large paxillin complexes detach from the adhesions and have been detected by the RICS analysis (29). In Fig. 10 we show the *B* map and the intensity images. Regions along the adhesions where *B* is

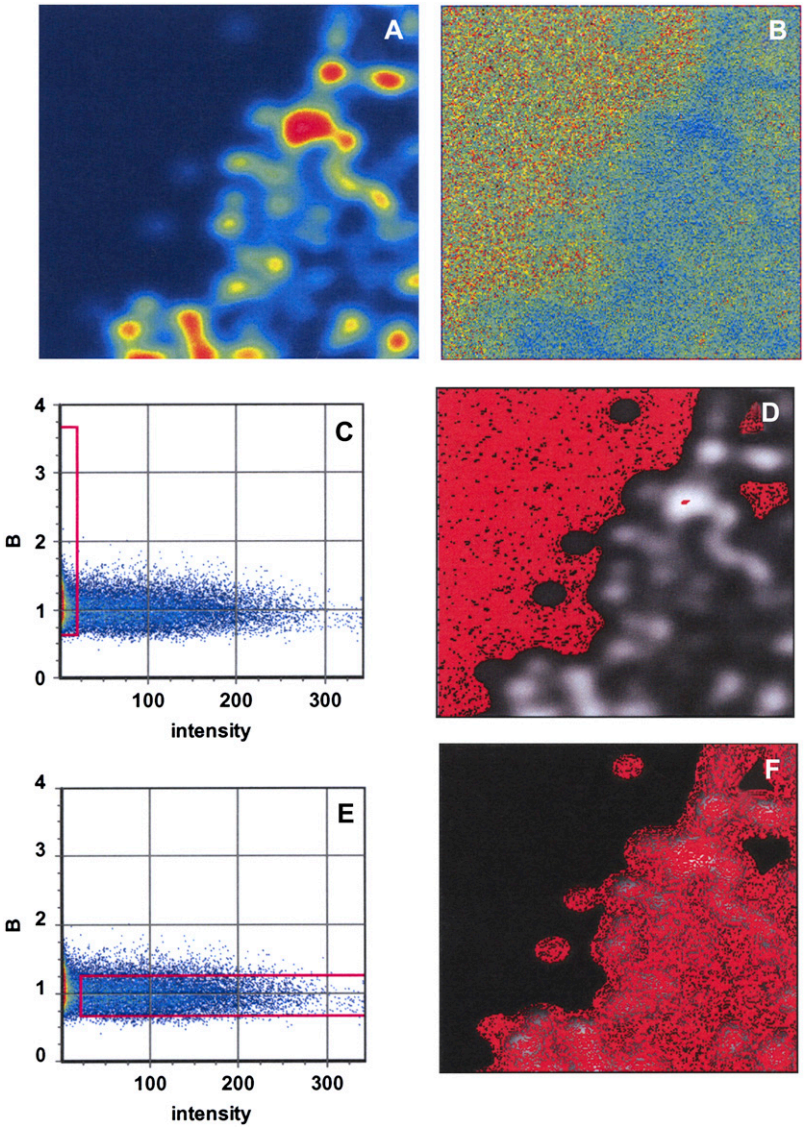

FIGURE 7 Fluorescent beads in a sea of 100 nM fluorescein. (*A*) The average image. (*B*) The *B* image. (*C*) Selecting points in the two-dimensional *B*-versus-intensity plot at low intensity and large *B* give the region in panel *D* red color where the beads are absent. (*E*) Selecting regions of the two-dimensional *B*-versus-intensity plot at large intensity and *B*-value at ~1 give the regions in panel *F* red color where the beads are present. One-hundred frames were collected for this measurement. Bleaching artifacts were corrected using the high-pass filter procedure. The image size is 11.2 μm × 11.2 μm.

large are identified from the *B* histogram and shown in red in Fig. 10 *D*. These regions correspond to the disassembling parts of the adhesions as identified by the decrease of intensity in the image stack. The image series was corrected for slow variations of the intensity and photobleaching using the algorithms described in Materials and Methods. These observations reveal a novel heterogeneity in aggregation state, at very high resolution, along the axis of a single adhesion in a live cell. We have measured >30 cells on several different days. In these cells, there are many adhesions. Some of the adhesions disassemble with a characteristic dynamics, as shown in Fig. 10.

DISCUSSION

The N&B analysis provides a measurement of the apparent brightness and number of molecules in every pixel of an image. This analysis requires an image stack of a minimum of 10–20 images, depending on intensity, to provide the values of the average and variance at each pixel used to calculate *N* and *B*. These parameters are related to the true number of particles and true brightness of the fluctuating particles according to the relationships presented in this article. For samples in solution, it is possible to extract the true values from the apparent values if we measure the variance of the detector. In the case of a detector operating in the photon-counting mode, the variance of the detector is equal to the intensity. We will discuss in a separate article how to obtain the maps of number of molecules and brightness for a detector operating in the analog mode, which includes most of the commercial laser-scanning confocal instruments and the camera systems.

Identification of immobile fraction

The N&B analysis can separate the mobile from the immobile fraction in an image. The *B*-value is unity for pixels

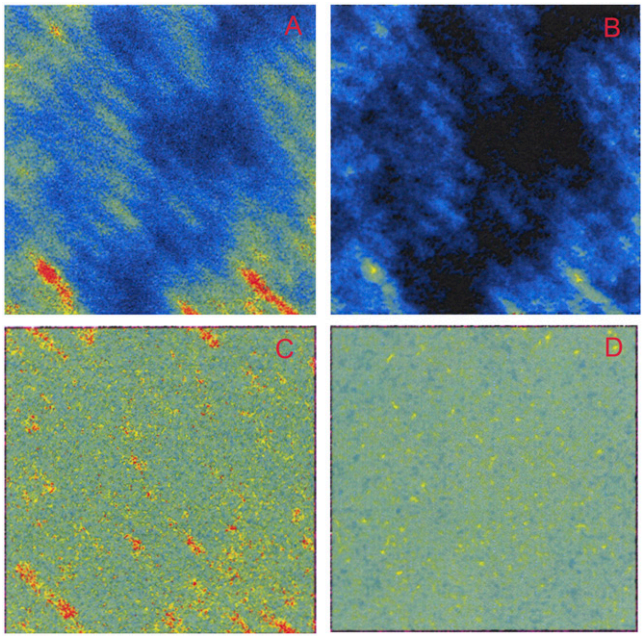

FIGURE 8 Fluorescent beads (fixed) in solution of 100 nM fluorescein. The entire slide was slowly moved using a piezo stage. The beads appear as elongated in the direction of the stage motion (*A*). The *B* image shown in panel *C* shows that motion produces value of *B* at the pixels of the beads larger than the value at the pixels where only the fluorescein is present. After immobile fraction removal using the high-pass filter method, the average intensity still shows a shadow of the beads (*B*). However, this shadow is very weak and the *B* image (*D*) appears uniform after the removal of the motion artifact. The image size is 11.2 μm $\times$ 11.2 μm.

with immobile particles while it is >1 if the particles are fluctuating. The value of *B* is equal to one plus the true brightness of the particle (for a photon-counting detector). Once the brightness is known, the number of particles (provided they are mobile) can be calculated by the ratio of the intensity to the brightness.

The N&B analysis cannot resolve a mixture of species of different brightness that reside in a single pixel. However, in an image, if there is localization of clusters of particles, then the brightness at these pixels could be large and easily recognizable in the *B* image. In addition, the values of *B* extracted from these mixtures represents the weighted average aggregation.

Origin of the intensity fluctuations

The N&B analysis only works if there are fluctuations. The fluctuations could arise from diffusion in and out of the observation volume, binding and unbinding to an immobile or slowly moving cellular feature, or any other process that cause a variation of the intensity in a pixel, e.g., a conformational transition or binding-unbinding process that produces an intensity fluctuation. In these cases, the *B*-value depends on the difference in intensity between the two states of the system. The *N*-value is proportional to the number of elements displaying intensity fluctuations.

Pixel dwell time

The pixel dwell time should always be smaller than the characteristic decay time of the fluctuations; otherwise the amplitude of the fluctuation will decrease. A very long pixel integration time (longer that the decay time of the fluctuations) reduces the variance. As a consequence of not using the appropriate sampling time, particles will appear dimmer and in larger number.

B and *N* image and one-dimensional and two-dimensional histograms

We present our data in the form of the *B* and *N* images and as one-dimensional histograms or two-dimensional histograms of *N* versus *B*, or *B* versus intensity. By selecting portions of these histograms, points in the image corresponding to regions of different brightness or number of particles can be identified. This is particularly useful for identifying molecular aggregates in the cell. Note that the *B* image is very different than the intensity image and it provides a method to display contrast based on the brightness of molecules, independently of their number.

Accuracy of the method

For particles in solutions, we find that the N&B analysis accurately calculates the true number of particles and brightness as recovered by the PCH analysis. For molecules in cells, the N&B analysis also provides accurate values for the true *n* and ε in regions of the cell where there are no immobile fractions. In the presence of immobile fraction, *n* and ε are undefined. The value of ε (Eq. 3) is independent of the number of particles. The only requirement is that the ratio between the variance and the intensity remain constant. At very large count rates, this ratio tends to decrease due to saturation effects of the photon-counting detector. The count rate at which the nonlinear regime is reached depends on the kind of detector used. For the photomultiplier detector used in this work, the value of the intensity at which the *B* falls to <1 for the EGFP sample 1 is $\sim$10 MHz. We also tested the avalanche photodiode detectors we have in our systems. The deviation from the unity value due to saturation starts at $\sim$1–2 MHz.

Effect of the number of frames

We also studied the effect of the number of frames necessary for the determination of *B* and *N*. For the conditions of our experiments we found that a minimum of $\sim$10–20 frames is necessary to determine the brightness and number of particles and to be capable of showing the location of molecular

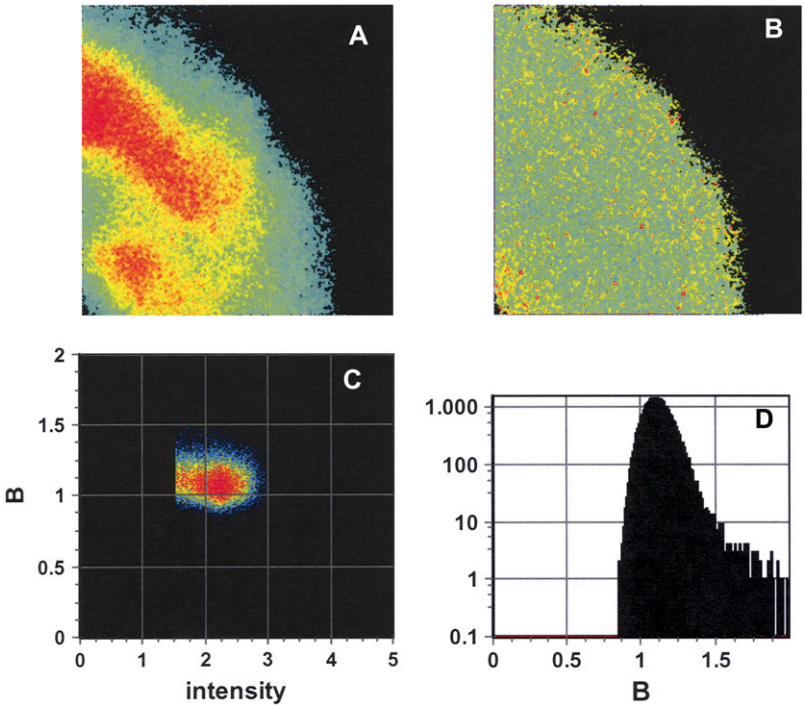

FIGURE 9 (*A*) Average image of a CHO-K1 cell transfect with EGFP. (*B*) The *B* image. (*C*) Two-dimensional histogram of the *B*-values versus intensity. A threshold at 1.5 counts was applied to this image to delete all points outside the cell from the analysis. The histogram in panel *C* is elongated due to the change in cell thickness. However, the *B*-value is relatively constant and >1. The brightness calculated for this cell is 3810 count/s/m. Calibration done at the same laser power for EGFP in solution shows brightness of 3960 counts/s/molecule. The histogram of the *B*-values (*D*) shows that the pixel distribution is relatively well defined. Forty frames were acquired for this measurement. The image size is 7.8 μm × 7.8 μm.

aggregates. However, since the error in the determination of the average and the variance decreases as the square-root of the number of independent measurements, the larger the number of frames, the better the resolving power of the method. Using a laser-scanning microscope, 10–20 images can be acquired in few seconds, providing a time resolution for the determination of protein aggregates sufficient to determine protein aggregation in response to external stimuli.

The spatial filter

When few counts are available in a pixel, statistical fluctuations tend to give noisy N&B images. The spatial filter method further improves the precision of the determination of N and B, since neighbor pixels are used to determine the B and N parameters, thereby increasing the statistics. The particular spatial filter used (the median filter) does not decrease the spatial resolution. On the contrary, it tends to sharpen the image. One important consideration is to avoid artificial clustering of points with a given brightness, which could be confused with regions of protein aggregation. For this reason the selection of a proper spatial filter is paramount.

Difference between $G(0)$ and extrapolated $G(0)$

One alternative approach to measure the number of particles in a cell is to use the inverse of the $G(0)$ term derived by FCS. In this context, the $G(0)$ term is the extrapolated $G(\tau)$ term when $\tau \rightarrow 0$. The advantage of using the extrapolated $G(0)$ term is that this term is not affected by the detector shot noise since the detector noise is uncorrelated. Instead, the N&B analysis uses the $G(0)$ term. For this reason we must know the detector variance to extract the brightness and number of particles.

The illumination profile

We showed that in a cell with varying thickness (like that shown in Fig. 9) the brightness is constant in the cell, including the cell borders; but the number of particles changes with cell thickness. Although this change in the number of particles at the cell borders is ''expected,'' we need to discuss under which conditions the brightness will appear to be constant. The measured brightness ultimately depends on the laser power. If the particles are spread in a volume in which the laser illumination is changing (the profile of illumination), the molecular brightness is weighted according to the square of the laser illumination profile (Eq. 3). This weighting is given by

$$\gamma = \int PSF^2(r)dr^3 / \int PSF(r)dr^3,$$

where $PSF(r)$ is the illumination profile. For an illumination profile given by a three-dimensional Gaussian shape, the factor $\gamma = 0.3536$, and for the Gaussian-Lorentzian shape, $\gamma = 0.076$ (22).

This is the same consideration used to introduce the factor γ in the $G(0)$ FCS expression (24). When we divide the brightness by the average intensity to calculate the number of molecules, the apparent number of molecules must be

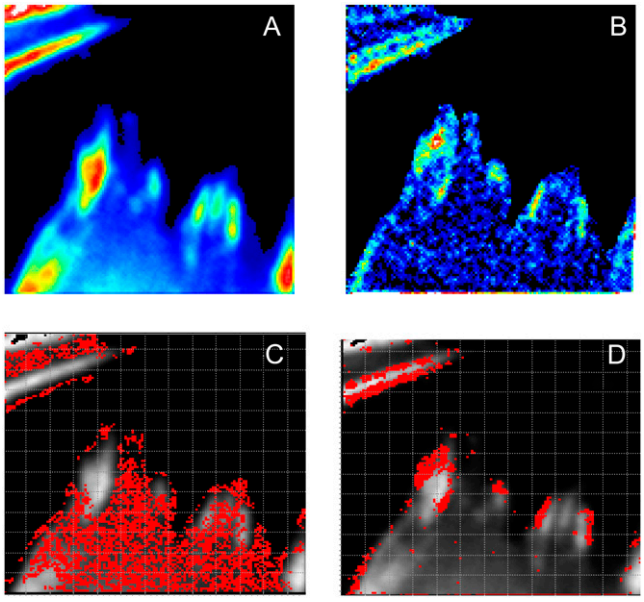

FIGURE 10 Paxillin-EGFP in CHO-K1 cells. (*A*) Average intensity. Paxillin accumulates at focal adhesions. (*B*) The *B* image shows that the larger values of *B* are seen at the borders of some adhesions. (*C*) Using the two-dimensional histogram of *B* versus intensity, all points with brightness of 1150 counts/s/molecules (corresponding to EGFP monomers were selected. These points accumulate in the cytosol. In panel *D*, all pixels with brightness of 11,500 counts/s/molecule were selected. These pixels accumulate at the border of the adhesions. Four-hundred frames were collected for this measurement. Motion artifacts were corrected using the high-pass filter procedure. The image size is 31 μm $\times$ 31 μm.

divided by the γ-factor to obtain the concentration. In other words, in line of what is done in the FCS field, we do not correct or normalize (to the center of the illumination profile) the value of the brightness but we use the γ-factor to calculate the true number of particles in the volume of illumination.

Since we have obtained equal brightness across the cell in our experiments with EFGP in the cytosol (Fig. 9), it implies that even at the cell borders the spatial distribution of the laser intensity is sampled enough not to appreciably modify the factor γ. If the particles are confined to the membrane (this is not the case of EGFP), they will appear brighter with respect to the same particles uniformly distributed in three dimensions. In effect, in Fig. 9 there is a slight tendency to larger apparent values of the *B* parameter toward the cell borders.

Bleaching effects

The effect of bleaching and of slowly moving bright features was also studied. Bleaching of immobile fractions or cell motion increases the variance. Therefore, moving features appear brighter. The trend due to bleaching can be subtracted using a high-pass filter, and restoring the value of the average intensity in each pixel. This procedure was applied to effectively remove the movement artifact in samples containing bright beads. The only requirement for this procedure to work is that the changes in intensity due to movement or bleaching must be slower than the particle fluctuations.

Visualization of the location of molecular aggregates

The application of the N&B analysis to cells with large aggregates shows the size and location of protein aggregates with very high resolution (pixel resolution). In the case of the paxillin protein binding and unbinding to the adhesions, we were able to identify the regions where monomers are the prevalent population (the cytosolic part) from other regions of the adhesions and (disassembling edges) where bright paxillin clusters are responsible for the fluctuations. The identification of brightness with molecular aggregates is based on the hypothesis that the interactions in the aggregates do not modify the molecular fluorescence. Of course, if quenching of the molecular components occurs, the N&B analysis will report an incorrect value for the aggregation number. In this case, it will be useful to complement the intensity fluctuation analysis with fluorescence lifetime data. We have performed independent determination of lifetime of the paxillin aggregates in cells, and we have not noticed reduction of the lifetime at adhesions.

CONCLUSIONS

The N&B analysis is a logical evolution of the work on the determination of dynamical processes in cell using microscope images. While the various image correlation techniques exploit the time correlation of the fluctuations to obtain the timescale of cellular processes, the N&B analysis exploits the amplitude fluctuations to obtain information on particle brightness and number. The brightness parameters can then be used to determine to aggregation of particles, which is a relevant parameter in biophysical studies. Since the brightness is independent of the number of molecules, the *B* images provide a new mechanism of contrast. Although in this article we presented only single channel data (one color), the method can be extended to multiple colors and multidimensional parameters. We have shown applications of the N&B method to relevant biological systems. There are many problems in cell biology that will benefit from this technique. The N&B method is a computational method, and it does not require any special hardware. We have demonstrated its use in the two-photon excitation microscope with photon-counting detectors. However, if the frame rate could be made large enough or the exposure times of cameras can be made short enough, commonly available cameras can be used with this technique. The N&B approach does not requires a special sequence of pixel acquisition and it should be applicable also to images obtained with the spinning-disk confocal method.

These studies were supported in part by the Cell Migration Consortium grant No. U54 GM64346 (to M.D., R.D., A.H., and E.G.) and National Institutes of Health grant No. NIH-P41-RRO3155 (to E.G.).

REFERENCES

1. Wiseman, P. W., C. M. Brown, D. J. Webb, B. Hebert, N. L. Johnson, J. A. Squier, M. H. Ellisman, and A. F. Horwitz. 2004. Spatial mapping of integrin interactions and dynamics during cell migration by image correlation microscopy. *J. Cell Sci.* 117:5521–5534.
2. Brown, C. M., and N. O. Petersen. 1998. An image correlation analysis of the distribution of clathrin associated adaptor protein (AP-2) at the plasma membrane. *J. Cell Sci.* 111:271–281.
3. Chen, Y., J. D. Muller, P. T. So, and E. Gratton. 1999. The photon counting histogram in fluorescence fluctuation spectroscopy. *Biophys. J.* 77:553–567.
4. Muller, J. D., Y. Chen, and E. Gratton. 2000. Resolving heterogeneity on the single molecular level with the photon-counting histogram. *Biophys. J.* 78:474–486.
5. Chen, Y., L. N. Wei, and J. D. Muller. 2003. Probing protein oligomerization in living cells with fluorescence fluctuation spectroscopy. *Proc. Natl. Acad. Sci. USA.* 100:15492–15497.
6. Chen, H., H. L. Puhl 3rd, S. V. Koushik, S. S. Vogel, and S. R. Ikeda. 2006. Measurement of FRET efficiency and ratio of donor to acceptor concentration in living cells. *Biophys. J.* 91:L39–L41.
7. Takanishi, C. L., E. A. Bykova, W. Cheng, and J. Zheng. 2006. GFP-based FRET analysis in live cells. *Brain Res.* 1091:132–139.
8. Meyer, B. H., J. M. Segura, K. L. Martinez, R. Hovius, N. George, K. Johnsson, and H. Vogel. 2006. FRET imaging reveals that functional neurokinin-1 receptors are monomeric and reside in membrane microdomains of live cells. *Proc. Natl. Acad. Sci. USA.* 103:2138–2143.
9. Brumbaugh, J., A. Schleifenbaum, A. Gasch, M. Sattler, and C. Schultz. 2006. A dual parameter FRET probe for measuring PKC and PKA activity in living cells. *J. Am. Chem. Soc.* 128:24–25.
10. Wichmann, O., J. Wittbrodt, and C. Schultz. 2006. A small-molecule FRET probe to monitor phospholipase A2 activity in cells and organisms. *Angew. Chem. Int. Ed. Engl.* 45:508–512.
11. Gertler, A., E. Biener, K. V. Ramanujan, J. Djiane, and B. Herman. 2005. Fluorescence resonance energy transfer (FRET) microscopy in living cells as a novel tool for the study of cytokine action. *J. Dairy Res.* 72:14–19.
12. Looger, L. L., S. Lalonde, and W. B. Frommer. 2005. Genetically encoded FRET sensors for visualizing metabolites with subcellular resolution in living cells. *Plant Physiol.* 138:555–557.
13. Kahn, E., A. Vejux, D. Dumas, T. Montange, F. Frouin, V. Robert, J. M. Riedinger, J. F. Stoltz, P. Gambert, A. Todd-Pokropek, and G. Lizard. 2004. FRET multiphoton spectral imaging microscopy of 7-ketocholesterol and Nile Red in U937 monocytic cells loaded with 7-ketocholesterol. *Anal. Quant. Cytol. Histol.* 26:304–313.
14. Ballestrem, C., and B. Geiger. 2005. Application of microscope-based FRET to study molecular interactions in focal adhesions of live cells. *Methods Mol. Biol.* 294:321–334.
15. Clayton, A. H., N. Klonis, S. H. Cody, and E. C. Nice. 2005. Dual-channel photobleaching FRET microscopy for improved resolution of protein association states in living cells. *Eur. Biophys. J.* 34:82–90.
16. Duncan, R. R., A. Bergmann, M. A. Cousin, D. K. Apps, and M. J. Shipston. 2004. Multi-dimensional time-correlated single photon counting (TCSPC) fluorescence lifetime imaging microscopy (FLIM) to detect FRET in cells. *J. Microsc.* 215:1–12.
17. Zal, T., and N. R. Gascoigne. 2004. Photobleaching-corrected FRET efficiency imaging of live cells. *Biophys. J.* 86:3923–3939.
18. Chen, Y., J. D. Mills, and A. Periasamy. 2003. Protein localization in living cells and tissues using FRET and FLIM. *Differentiation.* 71:528–541.
19. Tramier, M., T. Piolot, I. Gautier, V. Mignotte, J. Coppey, K. Kemnitz, C. Durieux, and M. Coppey-Moisan. 2003. Homo-FRET versus hetero-FRET to probe homodimers in living cells. *Methods Enzymol.* 360: 580–597.
20. Gautier, I., M. Tramier, C. Durieux, J. Coppey, R. B. Pansu, J. C. Nicolas, K. Kemnitz, and M. Coppey-Moisan. 2001. Homo-FRET microscopy in living cells to measure monomer-dimer transition of GFP-tagged proteins. *Biophys. J.* 80:3000–3008.
21. Gadella, T. W., Jr., G. N. van der Krogt, and T. Bisseling. 1999. GFP-based FRET microscopy in living plant cells. *Trends Plant Sci.* 4:287–291.
22. Berland, K. M., P. T. So, and E. Gratton. 1995. Two-photon fluorescence correlation spectroscopy: method and application to the intracellular environment. *Biophys. J.* 68:694–701.
23. Qian, H., and E. L. Elson. 1990. Distribution of molecular aggregation by analysis of fluctuation moments. *Proc. Natl. Acad. Sci. USA.* 87: 5479–5483.
24. Palmer, A. G., and N. L. Thompson. 1987. Molecular aggregation characterized by high order autocorrelation in fluorescence correlation spectroscopy. *Biophys. J.* 52:257–270.
25. Elson, E. L., and W. W. Webb. 1975. Concentration correlation spectroscopy: a new biophysical probe based on occupation number fluctuations. *Annu. Rev. Biophys. Bioeng.* 4:311–334.
26. Elson, E. L, and D. Magde. 1974. Fluorescence correlation spectroscopy. I. Conceptual basis and theory. *Biopolymers.* 13:1–27.
27. Schwille, P., J. Korlach, and W. W. Webb. 1999. Molecular dynamics in living cells observed by fluorescence correlation spectroscopy with single-molecule sensitivity on cell and model membranes. *Cytometry.* 36:176–182.
28. Digman, M. A., C. M. Brown, P. Sengupta, P. W. Wiseman, A. R. Horwitz, and E. Gratton. 2005. Measuring fast dynamics in solutions and cells with a laser scanning microscope. *Biophys. J.* 89:1317–1327.
29. Digman, M. A., M. C. Brown, A. R. Horwitz, W. W. Mantulin, and E. Gratton. 2007. Paxillin binding dynamics across adhesions measured by correlation spectroscopy. *Biophys. J.* In press.